An Improved Low-Complexity Model Predictive Direct Power Control With Reduced Power Ripples Under Unbalanced Grid Conditions

Xiaohong Ran, *Member, IEEE*, Bo Xu, Kaipei Liu, and Jiahao Zhang

***Abstract*—This article proposes an improved low-complexity model predictive direct power control (LC-MPDPC) along with reduced power ripples. Different from those MPDPC methods under balanced grid voltage conditions, both the design and implication of MPDPC under unbalanced grid conditions are further studied. In the proposed MPDPC, to reduce the computational burden of the controller, an improved LC-MPDPC based on the extended reactive *pq* theory is proposed. Only one prediction is needed to select the next voltage vector. Besides, the defined cost function under balanced grid conditions cannot obtain the minimized value if the unbalanced grid conditions occur. Accordingly, a new power error is defined, which is described analytically in the optimal model. With the proposed LC-MPDPC, a negative conjugate of the new defined complex power is selected as the control variable, and an improved modulation for the LC-MPDPC is presented to ensure the best voltage and calculate the optimal duration under unbalanced grid conditions. Compared with prior MPDPC, the proposed LC-MPDPC obtains much lower power ripples and grid current total harmonic distortion, and further, it offers a fast dynamic response and robustness. The effectiveness of the proposed LC-MPDPC is evaluated and validated by the experimental results.**

***Index Terms*—Extended reactive *pq* power theory, low-complexity model predictive direct power control (LC-MPDPC), unbalanced grid conditions.**

I. Introduction

SIGNIFICANT merits of three-phase pulsewidth modulation (PWM) rectifier including high power factor, bidirectional power flow, and low input current harmonic distortion have made them a viable solution for the renewable energy system [1], [2], voltage source converter-based system [3], [4], uninterruptible power supply [5], and microgrids [6]. Nevertheless, the increasing penetration level of the renewable energy into power grid together with the impact of nonideal or unbalanced grid conditions on the rectifiers have called for advanced control methods for PWM rectifiers.

In the technical literature, voltage-oriented control (VOC) [7], [8], and direct power control (DPC) [9]–[11] are the two well-known methods for the control of PWM rectifiers. VOC is a relatively mature control method, which decomposes the grid current into active power and reactive power components in the synchronous reference frame. The voltage vector reference is obtained by using the proportional–integral (PI) controllers. VOC demonstrates an acceptable performance, but its dynamic performance is limited by the bandwidth of its inner current control loops [12]. In DPC, the reference voltage vector is directly selected from a predefined switching table, and which is based on active and reactive power error signs. DPC does not require an inner current control loop and PWM block. Accordingly, it offers the fast dynamic response with a simple control structure. However, DPC highly depends on its predefined switching table and sampling frequency.

Due to the superior control performance, simplicity, the fast response of the model predictive control (MPC), it has been widely exploited in the control of power converters. Considering the merits and potential applications of MPC, it is valuable for the control of power converters and electric machines. On this front, the MPC in [13] is applied for torque control of a permanent magnet synchronous motor. In [14], MPC is used for dynamic performance improvement of ac/dc converter. Distributed MPC is used for a back-to-back converter [15] to reduce the computational burden of the controllers. In [16], the matrix converter is controlled by finite control set MPC (FCS-MPC). Among these MPC methods, the FCS-MPC is a highly effective method as it takes the discrete nature of power converters into account and results in optimal voltage vector. Taking model predictive power control (MPPC) as an example, the principle of selecting voltage vectors is to minimize the difference between references and predicted values of active and reactive powers. Compared with table-based DPC, the vector that is selected using FCS-MPC is effective for reducing power ripples. In [17], by exploiting MPC, a nonzero vector and a zero vector are used within each control period to obtain much lower power ripples while maintaining the simplicity and robustness of the controller.

Manuscript received March 19, 2021; revised July 3, 2021 and October 2, 2021; accepted November 20, 2021. Date of publication December 1, 2021; date of current version January 19, 2022. This work was supported in part by the National Natural Science Foundation of China under Grant 51607125 and in part by Hubei Natural Science Foundation under Grant 2017CFB521. Recommended for publication by Associate Editor P. Mattavelli. *(Corresponding author: Bo Xu.)*

Xiaohong Ran is with the School of Electrical Engineering and Automation, Wuhan University, Wuhan 430072, China, and also with the School of Electrical and Computer Engineering, Georgia Institute of Technology, Atlanta, GA 30332 USA (e-mail: xhran@whu.edu.cn).

Bo Xu, Kaipei Liu, and Jiahao Zhang are with the School of Electrical Engineering and Automation, Wuhan University, Wuhan 430072, China (e-mail: 2016202070016@whu.edu.cn; kpliu@whu.edu.cn; 2019282070110@whu.edu.cn).

Color versions of one or more figures in this article are available at https://doi.org/10.1109/TPEL.2021.3131794.

Digital Object Identifier 10.1109/TPEL.2021.3131794

Recently, a multiple-vector-based MPC [18] is presented for the permanent magnet synchronous motor drives. In [19] and [20], two MPPC methods are proposed for the rectifiers to realize capacitor voltage balancing and power ripples reduction. In the multivector MPPC, two nonzero vectors and a zero vector are exploited within each control period. All the aforementioned methods can improve the dynamic response and reduce its power reference tracking error. However, they impose more computational burden compared with the duty cycle control in MPC [17]. As an alternative, continuous control set model predictive control (CCS-MPC) is proposed, which offers an improvement in the total harmonic distortion (THD) of grid current and leads to a fixed switching frequency compared with FCS-MPC [21], although it is sensitive to parameter mismatches [22]. To obtain a small overshoot or a much lower THD, CCS-MPC employing multistep error tracking technique [23], and the multistep MPC [24] are proposed, both of which can achieve a reasonable steady-state performance. In addition, the uncertainty of the system model has an important impact on the design of the controller. Therefore, different MPC methods making use of disturbance observer [25], [26] are studied to enhance system robustness.

The FCS-MPC method is time-consuming as it minimizes a cost function to find the best voltage vector by evaluating six nonzero vectors and a zero vector. To address this problem, a single-vector-based low-complexity model predictive DPC (LC-MPDPC) [27] has been demonstrated. Moreover, double-vector LC-MPDPC is proposed in [28]. Both can simplify computational burden as they calculate the defined cost function only two times within each control period. For much lower power ripples and current THD, a three-vector-based LC-MPDPC is exploited for a doubly fed induction generator (DFIG) in [29] and [30]. Two merits of three-vector-based LC-MPDPC are included, i.e., low complexity and optimized voltage vector selection. These methods [27]–[29] are studied under balanced grid conditions; accordingly, the defined cost function under balanced grid conditions cannot obtain the minimized value if the unbalanced grid conditions occur. Furthermore, the LC-MPC is utilized in [30] under unbalanced grid voltages, but only single-vector-based LC-MPC is used.

As nonideal grid conditions are also presented, different methods are designed to obtain much lower power ripples and THD, and faster response under unbalanced grid conditions. To this end, an additional control loop is added into the control strategy in [31], and the power compensation is needed for better power quality of grid currents. To diminish the calculation complexity of the controller under unbalanced grid voltages, an extended instantaneous power theory (extended reactive *pq* power theory) is applied to MPC for control of a rectifier in [32] and [33]. Compared with the method in [31], the proposed scheme does not need any power compensation and tuning for the controller discussed in [32] and [33]. However, the proposed schemes in [32] and [33] are time-consuming. In this article, an improved multivector-based LC-MPDPC is elucidated, and the main contributions are as follows.

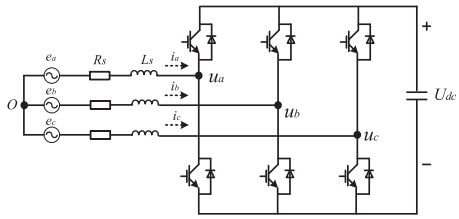

Fig. 1. Circuit diagram of a three-phase PWM converter.

1) The defined cost function from LC-MPDPC in [27]–[29] cannot obtain the minimized value if the unbalanced grid conditions occur; accordingly, a new complex vector using the extended reactive *pq* power theory is defined. A new power error is analyzed and also described analytically in the optimal model. A negative conjugate of new complex power is selected as the control variable, whereas the proposed method not only obtains minimized value of the cost function but also achieves good steady-state performance.
2) According to the characteristics of the single-vector LC-MPDPC in [30], under unbalanced grid voltages, an improved multivector LC-MPDPC using the extended reactive *pq* power theory is developed for much better control performance. Only one time is needed to predict the next voltage vector, as well as obtain much lower power ripples and the grid current THD under unbalanced grid conditions.
3) An improved LC-MPDPC is proposed under unbalanced grid to decrease calculation complexity, where the new modulation for LC-MPDPC is presented to ensure the best voltage and optimal duration under unbalanced grid conditions. Comparing with other MPDPC methods, the proposed method not only achieves good steady-state performance but also offers a fast dynamic response and robustness.

II. Model of AC/DC PWM Convector

The schematic diagram of a three-phase two-level PWM converter is shown in Fig. 1. The mathematical model of the rectifier in the stationary reference frame is expressed by

$$\boldsymbol{e} = R_s\boldsymbol{i} + L_s d\boldsymbol{i}/dt + \boldsymbol{u} \tag{1}$$

where $\boldsymbol{i}$, $\boldsymbol{e}$, and $\boldsymbol{u}$ represent the grid current, grid voltage, and converter voltage, respectively. R_s and L_s denote the equivalent series resistance and inductance of the interconnecting reactors. $\boldsymbol{e}$, $\boldsymbol{i}$, and $\boldsymbol{u}$ are defined as

$$\begin{aligned} \boldsymbol{e} &= 2/3 * (\boldsymbol{e}_a + \boldsymbol{a}\boldsymbol{e}_b + \boldsymbol{a}^2\boldsymbol{e}_c) \\ \boldsymbol{i} &= 2/3 * (\boldsymbol{i}_a + \boldsymbol{a}\boldsymbol{i}_b + \boldsymbol{a}^2\boldsymbol{i}_c) \\ \boldsymbol{u} &= s_{on}U_{\mathrm{dc}} \end{aligned} \tag{2}$$

where $\boldsymbol{a} = \exp(j2\pi/3)$, and $\boldsymbol{e}_s$ and $\boldsymbol{i}_s$ ($s = a, b, c$) are s-phase grid voltage and current, respectively. Moreover, ω is the angular frequency, and U_{dc} is the dc-link voltage. s_{on} is also defined as

$$s_{on} = 2(s_a + s_b\boldsymbol{e}^{j2\pi/3} + s_c\boldsymbol{e}^{-j2\pi/3})/3 \tag{3}$$

where s_i ($i = a, b, c$) is the switching state of the connected converter. $s_i = 1$ represents the upper bridge of phase i is ON and the lower bridge is OFF. $s_i = 0$ denotes the upper bridge of phase i is OFF and the lower bridge is ON.

According to the instantaneous power theory (*pq* power theory) introduced in [34], the complex power $\boldsymbol{S}_1$ is calculated using the grid voltage and current as follows:

$$\boldsymbol{S}_1 = 1.5(\boldsymbol{i}^* \boldsymbol{e}). \tag{4}$$

The active power P and reactive power Q are defined as

$$\begin{cases} P = \mathrm{Re}(\boldsymbol{S}_1) = 1.5\boldsymbol{i} \odot \boldsymbol{e} \\ Q = \mathrm{Im}(\boldsymbol{S}_1) = 1.5\boldsymbol{i} \otimes \boldsymbol{e} \end{cases} \tag{5}$$

where "$*$" is used to represent the conjugate of a complex vector. Moreover, $\odot$ and $\otimes$ denote the dot product and cross product of vector, respectively.

According to the definition of complex power, under balanced grid conditions, the derivative of negative conjugate for complex power $\boldsymbol{S}$ can be described as

$$\frac{d(-\boldsymbol{S}^*)}{dt} = -\frac{3}{2L_s}|\boldsymbol{e}|^2 + \frac{1}{L_s}(R_s + j\omega L_s)\boldsymbol{S}^* + \frac{3}{2L_s}\boldsymbol{u}\boldsymbol{e}^*. \tag{6}$$

Under unbalanced grid conditions, the derivative of negative conjugate for complex power $\boldsymbol{S}_n$ is described as

$$\begin{aligned} &\frac{d(-\boldsymbol{S}_n^*)}{dt} \\ &= -\frac{3}{2L_s}|\boldsymbol{e}|^2 + \frac{1}{L_s}(R_s\boldsymbol{S}_n^* + 1.5\omega L_s \boldsymbol{i}(\boldsymbol{e}')^*) + \frac{3}{2L_s}\boldsymbol{u}\boldsymbol{e}^* \end{aligned} \tag{7}$$

where $\boldsymbol{e}'$ represents the quadrature voltage, which lags $\boldsymbol{e}$ by 90 electrical degrees.

From (6) and (7), the derivative of negative conjugate for complex power under balanced grid conditions is different from that under unbalanced grid voltages. Accordingly, it is completely different from the design and implementation controller of LC-MPDPC under balanced and unbalanced grid conditions. At present, only single-vector LC-MPDPC under unbalanced grid conditions is presented in [30] for the DFIGs. In this article, we mainly focus on the controller design of multivector LC-MPDPC for ac/dc converter under unbalanced grid conditions.

From [20], the power compensation is added to obtain sinusoidal grid current under unbalanced grid conditions. To improve the steady-state performance and reduce the calculation burden of the controller, another complex vector $\boldsymbol{S}_2$ is proposed in [32], which is described as

$$\boldsymbol{S}_2 = 1.5(\boldsymbol{i}^* \boldsymbol{e}'). \tag{8}$$

In [32], the new reactive power Q^{nov} is defined as a real part of the complex power $\boldsymbol{S}_2$

$$Q^{\mathrm{nov}} = \mathrm{Re}(\boldsymbol{S}_2) = 1.5\boldsymbol{i} \odot \boldsymbol{e}'. \tag{9}$$

Hereafter, a new complex power described using the extended reactive *pq* power theory is defined as $\boldsymbol{S}_{\mathrm{new}} = P + jQ^{\mathrm{nov}}$. The definition of $\boldsymbol{S}_{\mathrm{new}}$ comprises the conventional active power P and new reactive power Q^{nov}.

Under unbalanced grid conditions, the grid voltage and grid current are described as the sum of the positive- and negative-sequence components as follows:

$$\begin{cases} \boldsymbol{e} = \boldsymbol{e}^+ + \boldsymbol{e}^- = \boldsymbol{e}_{dq}^+ \boldsymbol{e}^{j\omega t} + \boldsymbol{e}_{dq}^- \boldsymbol{e}^{-j\omega t} \\ \boldsymbol{i} = \boldsymbol{i}^+ + \boldsymbol{i}^- = \boldsymbol{i}_{dq}^+ \boldsymbol{e}^{j\omega t} + \boldsymbol{i}_{dq}^- \boldsymbol{e}^{-j\omega t} \end{cases} \tag{10}$$

where ($\boldsymbol{e}_{dq}{}^+$and $\boldsymbol{i}_{dq}{}^+$) and ($\boldsymbol{e}_{dq}{}^-$ and $\boldsymbol{i}_{dq}{}^-$) denote the positive- and negative-sequence components of grid voltage and current, respectively.

According to the extended *pq* power theory, $\boldsymbol{e}'$ is given by

$$\begin{aligned} \boldsymbol{e}' &= \boldsymbol{e}_{dq}^+ \boldsymbol{e}^{j(\omega t - \pi/2)} + \boldsymbol{e}_{dq}^- \boldsymbol{e}^{-j(\omega t - \pi/2)} \\ &= -j\boldsymbol{e}_{dq}^+ \boldsymbol{e}^{j\omega t} + j\boldsymbol{e}_{dq}^- \boldsymbol{e}^{-j\omega t} = -j\boldsymbol{e}^+ + j\boldsymbol{e}^-. \end{aligned} \tag{11}$$

Based on (8)–(11), under unbalanced grid conditions, active power P and new reactive power Q^{nov} are described as

$$\begin{aligned} P &= 1.5\mathrm{Re}(\boldsymbol{i}^* \boldsymbol{e}) \\ &= 1.5\mathrm{Re}\left[(\boldsymbol{i}_{dq}^+ \boldsymbol{e}^{j\omega t} + \boldsymbol{i}_{dq}^- \boldsymbol{e}^{-j\omega t})^* (\boldsymbol{e}_{dq}^+ \boldsymbol{e}^{j\omega t} + \boldsymbol{e}_{dq}^- \boldsymbol{e}^{-j\omega t})\right] \end{aligned} \tag{12}$$

$$\begin{aligned} Q^{\mathrm{nov}} &= 1.5\mathrm{Re}(\boldsymbol{i}^* \boldsymbol{e}') = 1.5\mathrm{Re}(\boldsymbol{i}^* \boldsymbol{e}(t - T_s/4)) \\ &= 1.5\mathrm{Re}\left[(\boldsymbol{i}_{dq}^+ \boldsymbol{e}^{j\omega t} + \boldsymbol{i}_{dq}^- \boldsymbol{e}^{-j\omega t})^* (-j\boldsymbol{e}_{dq}^+ \boldsymbol{e}^{j\omega t} + j\boldsymbol{e}_{dq}^- \boldsymbol{e}^{-j\omega t})\right] \end{aligned} \tag{13}$$

where T_s is the time period of the grid voltage.

Accordingly, the real power P and new reactive power Q^{nov} are expressed as

$$\begin{cases} P = P_0 + P_{c2}\cos(2\omega t) + P_{s2}\sin(2\omega t) \\ Q^{\mathrm{nov}} = Q_0^{\mathrm{nov}} + Q_{c2}^{\mathrm{nov}}\cos(2\omega t) + Q_{s2}^{\mathrm{nov}}\sin(2\omega t) \end{cases} \tag{14}$$

in which

$$\begin{bmatrix} P_0 = \frac{3}{2}(\boldsymbol{i}_{dq}^+ \odot \boldsymbol{e}_{dq}^+ + \boldsymbol{i}_{dq}^- \odot \boldsymbol{e}_{dq}^-) \\ P_{c2} = \frac{3}{2}(\boldsymbol{i}_{dq}^+ \odot \boldsymbol{e}_{dq}^- + \boldsymbol{i}_{dq}^- \odot \boldsymbol{e}_{dq}^+) \\ P_{s2} = \frac{3}{2}(\boldsymbol{i}_{dq}^+ \otimes \boldsymbol{e}_{dq}^- - \boldsymbol{i}_{dq}^- \otimes \boldsymbol{e}_{dq}^+) \end{bmatrix} \tag{15}$$

and

$$\begin{bmatrix} Q_0^{\mathrm{nov}} = \frac{3}{2}(\boldsymbol{i}_{dq}^+ \otimes \boldsymbol{e}_{dq}^+ - \boldsymbol{i}_{dq}^- \otimes \boldsymbol{e}_{dq}^-) \\ Q_{c2}^{\mathrm{nov}} = \frac{3}{2}(-\boldsymbol{i}_{dq}^+ \otimes \boldsymbol{e}_{dq}^- + \boldsymbol{i}_{dq}^- \otimes \boldsymbol{e}_{dq}^+) \\ Q_{s2}^{\mathrm{nov}} = \frac{3}{2}(\boldsymbol{i}_{dq}^+ \odot \boldsymbol{e}_{dq}^- + \boldsymbol{i}_{dq}^- \odot \boldsymbol{e}_{dq}^+). \end{bmatrix} \tag{16}$$

Based on (15) and (16), $P_{c2} = Q_{s2}{}^{\mathrm{nov}}$ and $P_{s2} = -Q_{c2}{}^{\mathrm{nov}}$. Accordingly, eliminating P_{c2} and P_{s2} in P leads to removing $Q_{s2}{}^{\mathrm{nov}}$ and $Q_{c2}{}^{\mathrm{nov}}$ in Q^{nov}. Hence, simultaneous elimination of active power P and new reactive power Q^{nov} can be achieved, which simplifies the controller as described in Section III.

III. Principle of the Proposed LC-MPDPC

A. Control Objective

The PWM rectifier operates under unbalanced grid voltage conditions, which adversely impact the active power, reactive power, grid currents, and dc-side voltage of the rectifier. If the control target is to ensure constant active and reactive powers, then the grid currents would be highly distorted. A number of control objectives are proposed to deal with these problems

caused by unbalanced grid conditions, such as the cancelation of active power oscillation and reactive power ripple elimination, respectively, obtaining sinusoidal grid currents. In this article, under unbalanced grid conditions, the control objective of a PWM rectifier is to guarantee constant active power and generate sinusoidal grid currents. This can be achieved by avoiding any active power oscillation [32]. It means that the dc component of the active power P_0 is equal to the reference of the active power P^{ref}. Furthermore, the double-frequency components of the active power are equal to zero, i.e., $P_{c2} = P_{s2} = 0$. In this article, the dc component of new reactive power Q^{nov} is equal to zero to ensure unity power factor. Therefore, the control targets can be described as

$$\begin{bmatrix} P_0 = 1.5(\boldsymbol{i}_{dq}^{+} \odot \boldsymbol{e}_{dq}^{+} + \boldsymbol{i}_{dq}^{-} \odot \boldsymbol{e}_{dq}^{-}) = P^{\text{ref}} \\ P_{c2} = 1.5(\boldsymbol{i}_{dq}^{+} \odot \boldsymbol{e}_{dq}^{-} + \boldsymbol{i}_{dq}^{-} \odot \boldsymbol{e}_{dq}^{+}) = 0 \\ P_{s2} = 1.5(\boldsymbol{i}_{dq}^{+} \otimes \boldsymbol{e}_{dq}^{-} - \boldsymbol{i}_{dq}^{-} \otimes \boldsymbol{e}_{dq}^{+}) = 0 \\ Q_0^{\text{nov}} = 1.5(\boldsymbol{i}_{dq}^{+} \otimes \boldsymbol{e}_{dq}^{+} - \boldsymbol{i}_{dq}^{-} \otimes \boldsymbol{e}_{dq}^{-}) = 0 \end{bmatrix}. \tag{17}$$

The second equation and third one in (17) ensure no ripple exists in the active power. Based on (15) and (16), the ripples in reactive power are removed as well. The fourth equation in (17) ensures the unity power factor operation of the rectifier.

In the stationary frame, the proposed control objectives become equivalent to solving the following equations [32]:

$$\begin{bmatrix} P_0 = \frac{3}{4}(\boldsymbol{i} \odot \boldsymbol{e} + \boldsymbol{i}' \odot \boldsymbol{e}') = P^{\text{ref}} \\ k_1 = \boldsymbol{i} \odot \boldsymbol{e} - \boldsymbol{i}' \odot \boldsymbol{e}' = 0 \\ k_2 = \boldsymbol{i} \odot \boldsymbol{e}' + i' \odot \boldsymbol{e} = 0 \\ Q_0^{\text{nov}} = \frac{3}{4}(\boldsymbol{i} \odot \boldsymbol{e}' - \boldsymbol{i}' \odot \boldsymbol{e}) = 0 \end{bmatrix}. \tag{18}$$

The reference of the current vector is calculated by

$$\boldsymbol{i}^{\text{ref}} = -j\frac{2\boldsymbol{e}'}{3(\boldsymbol{e} \otimes \boldsymbol{e}')}P^{\text{ref}}. \tag{19}$$

According to the current reference in (19) and the definition of the active power and new reactive power, it is concluded that $P_{\text{new}}{}^{\text{ref}} = P^{\text{ref}}$ and $Q_{\text{new}}{}^{\text{ref}} = 0$ [32]. It means that the new power reference $P_{\text{new}}{}^{\text{ref}}$ is equal to the original power references P^{ref}. It does not require any additional power compensation. If the same control objective is considered using the *pq* power theory, the additional power compensation would be essential [20].

B. Principle of LC-MPDPC

The controller design for the rectifier under balanced grid conditions is greatly different from that under unbalanced grid voltages. To model the improved multivector LC-MPDPC under unbalanced grid conditions, first the derivatives of the complex powers $\boldsymbol{S}_1$ and $\boldsymbol{S}_2$ are described as

$$\begin{bmatrix} \frac{d\boldsymbol{S}_1}{dt} = \frac{1}{L_s}\left(1.5(|\boldsymbol{e}|^2 - \boldsymbol{u}^*\boldsymbol{e}) - R_s\boldsymbol{S}_1 - \omega L_s\boldsymbol{S}_2\right) \\ \frac{d\boldsymbol{S}_2}{dt} = \frac{1}{L_s}\left(1.5(\boldsymbol{e}^* - \boldsymbol{u}^*)\boldsymbol{e}' - R_s\boldsymbol{S}_2 + \omega L_s\boldsymbol{S}_1\right) \end{bmatrix}. \tag{20}$$

Accordingly, the derivative of the new defined complex power $\boldsymbol{S}_{\text{new}}$ is given by

$$\frac{d\boldsymbol{S}_{\text{new}}}{dt} = \text{Re}\left\langle \frac{d\boldsymbol{S}_1}{dt} \right\rangle + \text{Re}\left\langle \frac{d\boldsymbol{S}_2}{dt} \right\rangle. \tag{21}$$

Based on (20) and (21), the derivative of $-\boldsymbol{S}^*{}_{\text{new}}$ is given by

$$L_s\frac{d(-\boldsymbol{S}_{\text{new}}^*)}{dt} = -1.5|\boldsymbol{e}|^2 + 1.5(\text{Re}(\boldsymbol{u}^*\boldsymbol{e}) + j\text{Re}(\boldsymbol{e}^* - \boldsymbol{u}^*)\boldsymbol{e}') + (R_s + j\omega L_s)\boldsymbol{S}_{\text{new}}^*. \tag{22}$$

Hereafter, (22) is discretized as

$$(-\boldsymbol{S}_{\text{new}}^*)_u^{k+1} = (-\boldsymbol{S}_{\text{new}}^*)_0^{k+1} + \frac{3T_s}{2L_s}\left[(\boldsymbol{e}_\alpha\boldsymbol{u}_\alpha + \boldsymbol{e}_\beta\boldsymbol{u}_\beta) - j(\boldsymbol{u}_\alpha\boldsymbol{e}'_\alpha + \boldsymbol{u}_\beta\boldsymbol{e}'_\beta)\right] \tag{23}$$

where $(-\boldsymbol{S}_{\text{new}}{}^*)_0{}^{k+1}$ represents the natural response caused by the zero vector, which is given by

$$(-\boldsymbol{S}_{\text{new}}^*)_0^{k+1} = (-\boldsymbol{S}_{\text{new}}^*)^k + \frac{T_s}{L_s}\left\{-1.5|\boldsymbol{e}|^2 + (R_s + j\omega L_s)(\boldsymbol{S}_{\text{new}}^*)^k + j1.5(\boldsymbol{e}_\alpha\boldsymbol{e}'_\alpha + \boldsymbol{e}_\beta\boldsymbol{e}'_\beta)\right\} \tag{24}$$

where subscript "0" denotes the situation under which the zero vector is only exploited.

On the basis of (24), $\Delta(-\boldsymbol{S}_{\text{new}}{}^*)_0{}^{k+1}$ that is equal to $(-\boldsymbol{S}_{\text{new}}{}^{*\text{ref}})-(-\boldsymbol{S}_{\text{new}}{}^*)_0{}^{k+1}$ does not depend on the converter voltage $\boldsymbol{u}$. Accordingly, it can be interpreted as the natural response, and it is not controllable. The power error caused by the vector $\boldsymbol{u}$ can be described by

$$\begin{aligned}\Delta(-\boldsymbol{S}_{\text{new}}^*)_u^{k+1} &= (-\boldsymbol{S}_{\text{new}}^{*\text{ref}}) - (-\boldsymbol{S}_{\text{new}}^*)_u^{k+1} \\ &= \Delta(-\boldsymbol{S}_{\text{new}}^*)_0^{k+1} - \frac{3T_s}{2L_s}\left[(\boldsymbol{e}_\alpha\boldsymbol{u}_\alpha + \boldsymbol{e}_\beta\boldsymbol{u}_\beta) - j(\boldsymbol{u}_\alpha\boldsymbol{e}'_\alpha + \boldsymbol{u}_\beta\boldsymbol{e}'_\beta)\right]\end{aligned} \tag{25}$$

where the subscript "$\boldsymbol{u}$" represents the situation under which nonzero vector is utilized.

Based on (24) and (25), $\Delta(-\boldsymbol{S}_{\text{new}}{}^*)_0{}^{k+1}$ is the power error caused by zero vector, and it is calculated as

$$\Delta(-\boldsymbol{S}_{\text{new}}^*)_0^{k+1} = (-\boldsymbol{S}_{\text{new}}^{*\text{ref}}) - (-\boldsymbol{S}_{\text{new}}^*)^k - \frac{T_s}{L_s}\left\{-1.5|\boldsymbol{e}|^2 + (R_s + j\omega L_s)(\boldsymbol{S}_{\text{new}}^*)^k + j1.5(\boldsymbol{e}_\alpha\boldsymbol{e}'_\alpha + \boldsymbol{e}_\beta\boldsymbol{e}'_\beta)\right\}. \tag{26}$$

Equation (25) that defines the power error $\Delta(-\boldsymbol{S}_{\text{new}}{}^*)_u{}^{k+1}$ is the basis on which the proposed method is developed and will be discussed in Section IV.

IV. Proposed LC-MPDPC Method

Assuming that Δ_1 is equal to $(\boldsymbol{u}_\alpha\boldsymbol{e}_\beta\text{-}\boldsymbol{u}_\beta\boldsymbol{e}_\alpha)-(\boldsymbol{e}_\alpha\text{'}\boldsymbol{u}_\alpha+\boldsymbol{e}_\beta\text{'}\boldsymbol{u}_\beta)$, (25) is rewritten as

$$\begin{aligned}\Delta(-\boldsymbol{S}_{\text{new}}^*)_u^{k+1} &= (-\boldsymbol{S}_{\text{new}}^{*\text{ref}}) - (-\boldsymbol{S}_{\text{new}}^*)_u^{k+1} \\ &= \Delta(-\boldsymbol{S}_{\text{new}}^*)_0^{k+1} - 1.5T_s(j\Delta_1 + \boldsymbol{u}\boldsymbol{e}^*)/L_s.\end{aligned} \tag{27}$$

With respect to (27), new power error $\Delta(-\boldsymbol{S}_{\text{new}}{}^*)_u{}^{k+1}$ consists of three terms: the first term is the power error caused by the zero vector $\Delta(-\boldsymbol{S}_{\text{new}}{}^*)_0{}^{k+1}$, the second power variation is equal to $j1.5T_s\Delta_1/L_s$, and the third one is the power variation caused by the nonzero vector $3T_s\boldsymbol{u}\boldsymbol{e}^*/(2L_s)$.

If the exact values of $\boldsymbol{u}_\alpha$ and $\boldsymbol{u}_\beta$ were known, Δ_1 could be calculated. Based on (27), the controller could be designed by LC-MPDPC. Therefore, calculating $\boldsymbol{u}_\alpha$ and $\boldsymbol{u}_\beta$ plays a key role. Ideally, the total power error expressed by (27) should be zero. Therefore, by equating $\Delta(-\boldsymbol{S}_{\text{new}}{}^*)_u{}^{k+1}$ to zero, the magnitude of nonzero vectors u_α and $\boldsymbol{u}_\beta$ can be obtained by solving the following equation:

$$\Delta(-\boldsymbol{S}^*_{\text{new}})_u^{k+1} = \Delta(-\boldsymbol{S}^*_{\text{new}})_0^{k+1} - 1.5T_s(j\Delta_1 + \boldsymbol{u}\boldsymbol{e}^*)/L_s = 0. \tag{28}$$

To solve (28), two parameters are introduced, that is, the real and imaginary parts of power error caused by the zero vector are arranged as γ_1 and γ_2

$$\begin{cases} \gamma_1 = -P^{\text{ref}} + P^k - T_s(-\frac{3}{2L_s}|\boldsymbol{e}|^2 + \frac{R_s}{L_s}P^k + \omega Q^k_{\text{nov}}) \\ \gamma_2 = Q^{\text{ref}}_{\text{nov}} - Q^k_{\text{nov}} - T_s\left[\frac{3}{2L_s}(e^k_\alpha e'^k_\alpha + e^k_\beta e'^k_\beta)\right. \\ \quad \left. -\frac{R_s}{L_s}Q^k_{\text{nov}} + \omega P^k\right]. \end{cases} \tag{29}$$

Substituting (29) into (28), it can be obtained as

$$\begin{cases} 1.5T_s(e_\alpha u_\alpha + e_\beta u_\beta)/L_s = \gamma_1 \\ -1.5T_s(e'_\alpha u_\alpha + e'_\beta u_\beta)/L_s = \gamma_2. \end{cases} \tag{30}$$

According to Kramer's law, $\boldsymbol{u}_\alpha$ and $\boldsymbol{u}_\beta$ satisfying (28) are described as

$$\begin{cases} \boldsymbol{u}^{\text{opt}}_\alpha = \frac{2L_s}{3T_s}\frac{\gamma_1\boldsymbol{e}'_\beta + \gamma_2\boldsymbol{e}_\beta}{\boldsymbol{e}_\alpha\boldsymbol{e}'_\beta - \boldsymbol{e}'_\alpha\boldsymbol{e}_\beta} \\ \boldsymbol{u}^{\text{opt}}_\beta = -\frac{2L_s}{3T_s}\frac{\gamma_2\boldsymbol{e}_\alpha + \gamma_1\boldsymbol{e}'_\alpha}{\boldsymbol{e}_\alpha\boldsymbol{e}'_\beta - \boldsymbol{e}'_\alpha\boldsymbol{e}_\beta}. \end{cases} \tag{31}$$

Hereafter, $\boldsymbol{u}_\alpha{}^{\text{opt}}$ and $\boldsymbol{u}_\beta{}^{\text{opt}}$ are substituted in (27), which evolves to

$$\begin{aligned} \Delta(-\boldsymbol{S}^*_{\text{new}})_u^{k+1} &= (-\boldsymbol{S}^{*\text{ref}}_{\text{new}}) - (-\boldsymbol{S}^*_{\text{new}})_u^{k+1} \\ &= \gamma_1 + j\gamma_2 - j1.5T_s\Delta_2/L_s - 1.5T_s\boldsymbol{u}\boldsymbol{e}^*/L_s \end{aligned} \tag{32}$$

where $\Delta_2 = (\boldsymbol{u}_\alpha{}^{\text{opt}}\boldsymbol{e}_\beta\text{-}\boldsymbol{u}_\beta{}^{\text{opt}}\boldsymbol{e}_\alpha)\text{–}(\boldsymbol{e}_\alpha{}'\boldsymbol{u}_\alpha{}^{\text{opt}} + \boldsymbol{e}_\beta{}'\boldsymbol{u}_\beta{}^{\text{opt}})$.

Based upon (32), the real part γ_3 and imaginary part γ_4 of the power error caused by the zero vector and power variation that is $j1.5T_s\Delta_2/L_s$ are described as

$$\begin{cases} \gamma_3 = \gamma_1 \\ \gamma_4 = \gamma_2 - 1.5T_s\Delta_2/L_s. \end{cases} \tag{33}$$

According to the new power error described by (33), its corresponding amplitude and phase angle are expressed as

$$\begin{cases} \theta_2 = \text{atan}(\gamma_4/\gamma_3) \\ |b_{\text{new}}| = \text{sqrt}\left(\gamma_3^2 + \gamma_4^2\right). \end{cases} \tag{34}$$

Here, note that the power error vector $\boldsymbol{b}_{\text{original}}$ is under balanced grid conditions, which is different from power error $\boldsymbol{b}$ and $\boldsymbol{b}_{\text{new}}$ under unbalanced grid conditions. $\boldsymbol{b}_{\text{original}}$ is described as

$$\begin{aligned} \boldsymbol{b}_{\text{original}} = \Delta(-\boldsymbol{S}^*)_0^{k+1} &= (-\boldsymbol{S}^*)^{\text{ref}} - (-\boldsymbol{S}^*)^k \\ &-T_s[-1.5|\boldsymbol{e}|^2 + (R_s + j\omega L_s)\cdot\boldsymbol{S}^*]/L_s \end{aligned} \tag{35}$$

where power error vector $\boldsymbol{b}_{\text{original}} \neq \boldsymbol{b} \neq \boldsymbol{b}_{\text{new}}$. $\boldsymbol{b}$ and $\boldsymbol{b}_{\text{new}}$ are given in the following parts.

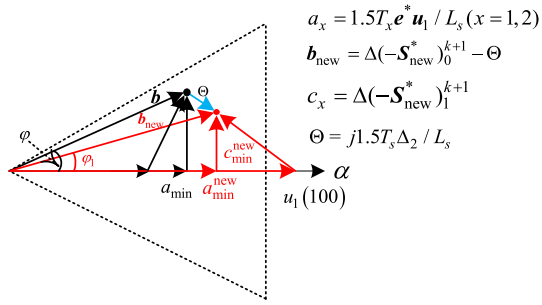

Fig. 2. Improved two-vector-based modulation method of LC-MPDPC.

Once optimal values of nonzero vectors $\boldsymbol{u}_\alpha$ and $\boldsymbol{u}_\beta$ are obtained, the controller is designed according to the principle of LC-MPDPC. To illustrate the proposed method in this article, three vectors are defined as

$$\begin{cases} \boldsymbol{a}_u = 1.5T_s\boldsymbol{e}^*\boldsymbol{u}/L_s \\ \boldsymbol{c}_u = \Delta(-\boldsymbol{S}^*_{\text{new}})_u^{k+1} \\ \boldsymbol{b}_{\text{new}} = \Delta(-\boldsymbol{S}^*_{\text{new}})_0^{k+1} - j1.5T_s\Delta_2/L_s. \end{cases} \tag{36}$$

The amplitude of vector $\boldsymbol{c}_u$ is described as

$$\begin{aligned} |\boldsymbol{c}_u| &= \left|(-\boldsymbol{S}^{*\text{ref}}_{\text{new}}) - (-\boldsymbol{S}^*_{\text{new}})_u^{k+1}\right| \\ &= \text{sqrt}\left[\left(-P^{\text{ref}} + P^{k+1}\right)^2 + \left(Q^{\text{ref}}_{\text{nov}} - Q^{k+1}_{\text{nov}}\right)^2\right]. \end{aligned} \tag{37}$$

From (37), the amplitude of vector $\boldsymbol{c}_u$ is equal to power error, which is considered as cost function for the LC-MPDPC.

A. Improved Two-Vector-Based LC-MPDPC

Two-vector-based LC-MPDPC, a nonzero vector and a zero vector are applied in every control period, is improved in this section. The LC-MPDPC scheme is carried out by two steps: best vector selection and duty cycle calculation. The selection principle of voltage vector is the same as that of MPDPC in [29]. Fig. 2 describes its improved modulation method. Under balanced grid voltages, the modulation method of two-vector LC-MPDPC is proposed in [28] and [29]. The power error $\boldsymbol{b}$ is in Sector I, the defined cost function can obtain the minimized value when $\boldsymbol{c}_{\text{min}}$ is vertical to $\boldsymbol{U}_1(100)$, and the φ is the angle between power error $\boldsymbol{b}$ and voltage $\boldsymbol{U}_1(100)$. However, under unbalanced grid conditions, the derivative of negative conjugate of complex power is greatly different from that under balanced grid conditions, which are described in (20)–(26). With the effect of unbalanced grid voltages, actual power error is changed to $\boldsymbol{b}_{\text{new}}$ with adding Θ on the basis of the power error $\boldsymbol{b}$, and $\Theta = j1.5T_s\Delta_2/L_s$. Basic power error $\boldsymbol{b} = \Delta(-\boldsymbol{S}_{\text{new}}{}^*)_0{}^{k+1}$ is shown in (24), and new power error is $\boldsymbol{b}_{\text{new}} = \boldsymbol{b}\text{–}\Theta$ under unbalanced grid voltages. As shown in Fig. 2, the smallest amplitude of $\boldsymbol{c}_x$ can be obtained when $\boldsymbol{c}_x$ is vertical to $\boldsymbol{u}_1$, that is, $\boldsymbol{c}_{\text{min}}{}^{\text{new}}$, and the nonzero vector is $\boldsymbol{a}_{\text{min}}{}^{\text{new}}$. Accordingly, optimal duration of $\boldsymbol{u}_1$ can be described as

$$t_{\text{new}} = \frac{|\boldsymbol{b}_{\text{new}}|\cos\varphi_1}{|1.5e^*a^{\text{new}}_{\text{min}}/L_s|} = \frac{L_s\,|\boldsymbol{b}_{\text{new}}|\cos\varphi_1}{|\boldsymbol{e}^*|\,|U_{\text{dc}}|} \tag{38}$$

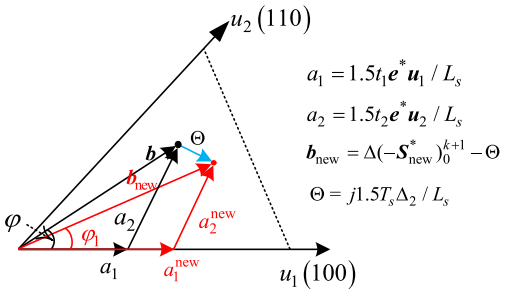

Fig. 3. Improved three-vector-based modulation method of LC-MPDPC.

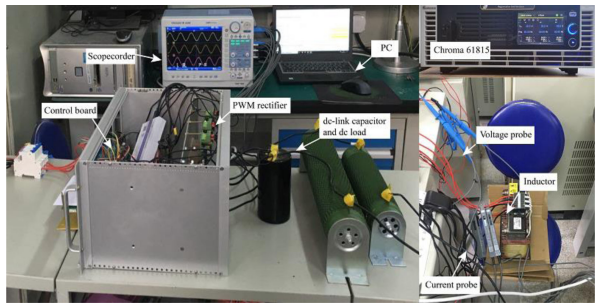

Fig. 4. Schematic diagram of the experimental setup.

where φ_1 is equal to $\theta_1+\theta_2$, θ_1 is the phase angle of grid voltage, and θ_2 is expressed by (34). If the vector $\boldsymbol{b}_{\text{new}}$ is in other sectors, the calculating process of the time durations t_1 and t_0 is similar. In addition, $\varphi = \theta_1 + \text{atan}(\gamma_{2/}\gamma_1)$.

Observed from the nonzero vector and duty cycle calculation, the proposed duty-cycle optimization-based LC-MPDPC is a better and easy method compared to conventional MPDPC methods in [20] and [32].

B. Improved Three-Vector-Based LC-MPDPC

To reduce the power error $\boldsymbol{b}_{\text{new}}$, an improved three-vector-based LC-MPDPC method is proposed under unbalanced grid conditions. In the proposed three-vector LC-MPDPC method, two adjacent nonzero vectors and a zero vector are utilized within every control period. The selection principle of voltage vectors is the same as that of MPDPC in [29]; moreover, the improved duty cycle calculation is stated in this section.

Fig. 3 demonstrates the improved three-vector modulation. Taking Sector I as an example, vectors $\boldsymbol{a}_1$ and $\boldsymbol{a}_2$ denote the power variations when $\boldsymbol{u}_1$ (100) and $\boldsymbol{u}_2$ (110) are used for the time intervals of t_{new1} and t_{new2}. Under balanced grid conditions, original power variable vectors are $\boldsymbol{a}_1$ and $\boldsymbol{a}_2$, and the power error vector $\boldsymbol{b}$ is followed. However, under unbalanced grid conditions, the power error is $\boldsymbol{b}_{\text{new}} = \boldsymbol{b}$–$\Theta$ not be $\boldsymbol{b}$. In proposed improved three-vector modulation, the new power variable vectors $\boldsymbol{a}_1{}^{\text{new}}$ and $\boldsymbol{a}_2{}^{\text{new}}$ are synthesized to follow error $\boldsymbol{b}_{\text{new}}$. From Fig. 3, in Sector I, the nonzero vectors are $\boldsymbol{u}_1$ and $\boldsymbol{u}_2$, and (39) can be obtained as

$$\frac{1.5t_{\text{new1}}\,|\boldsymbol{e}^*|\,|\boldsymbol{u}_1|\,/L_s}{\sin(\pi/3-\varphi_1)} = \frac{1.5t_{\text{new2}}\,|\boldsymbol{e}^*|\,|\boldsymbol{u}_2|\,/L_s}{\sin\varphi_1} = \frac{|\boldsymbol{b}_{\text{new}}|}{\sin(2\pi/3)} \tag{39}$$

where φ_1 is the angle between $\boldsymbol{b}_{\text{new}}$ and $\boldsymbol{u}_1$, and $|\boldsymbol{u}_1|$ and $|\boldsymbol{u}_2|$ are the amplitudes of $\boldsymbol{u}_1$ and $\boldsymbol{u}_2$, respectively.

The optimal time intervals for $\boldsymbol{u}_1$ and $\boldsymbol{u}_2$ can be obtained as

$$\begin{bmatrix} t_{\text{new1}} = \frac{2L_s|\boldsymbol{b}_{\text{new}}|}{\sqrt{3}|\boldsymbol{e}^*||U_{dc}|}\sin(\frac{\pi}{3}-\varphi) \\ t_{\text{new2}} = \frac{2L_s|\boldsymbol{b}_{\text{new}}|}{\sqrt{3}|\boldsymbol{e}^*||U_{dc}|}\sin\varphi \end{bmatrix} \tag{40}$$

where $|U_{\text{dc}}|$ is the amplitude of the dc-side voltage U_{dc}.

Accordingly, the duration of zero voltage vector is given by

$$t_0 = T_s - t_{\text{new1}} - t_{\text{new2}}. \tag{41}$$

TABLE I
TEST SYSTEM SPECIFICATIONS

Variable	Description	Value
Line voltage frequency	f	50 Hz
DC-side capacitor	C	4700 μF
Phase voltage (rms)	e	45 V
Load resistance	R_L	30 Ω
Sampling frequency	f_s	10 kHz
Filter inductance	L_s	12 mH
Equivalent resistance	R_s	0.04 Ω

From the aforementioned analysis, the proposed three-vector LC-MPDPC can theoretically reduce power error and provide a much better sinusoidal grid current compared to two-vector LC-MPDPC. Compared to other multivector MPDPC methods [20] and [32], the presented three-vector LC-MPDPC is a much simpler way and can obtain much better control performance, and it offers a fast dynamic response and robustness.

C. Time Delay Compensation

For the implementation of the improved LC-MPDPC method under unbalanced grid conditions, there is a one-step delay in digital signal controller caused by calculation [20], [27], [28], [32]. To eliminate the adverse impact of one-step delay, P and Q_{nov} are predicted at $(k+2)$th instant in the cost function expressed in (37). With values of $\Delta(-\boldsymbol{S}_{\text{new}}{}^*)_u$ and $\Delta(-\boldsymbol{S}_{\text{new}}{}^*)_0$ at $(k+2)$th instant, both of them are utilized to compute the amplitude and phase angle in (34) of power error. In addition, three vectors $\boldsymbol{a}_u$, $\boldsymbol{c}_u$, and $\boldsymbol{b}_{\text{new}}$ in (36) at $(k+2)$th instant rather than at $(k+1)$th instant are used for the best vector selection and optimal time calculation. More details about one-step delay can be found in [35].

V. EXPERIMENTAL STUDIES

In this section, experimental tests are conducted on a two-level three-phase PWM rectifier, shown in Fig. 4. The specifications of the test system are listed in Table I. The proposed algorithm is implemented on a DSP TMS320F28335 manufactured by Texas Instrument. The grid voltage is generated by a programmable ac source (Chroma 61815). The grid voltages/currents are displayed and recorded using YOKOGAWA

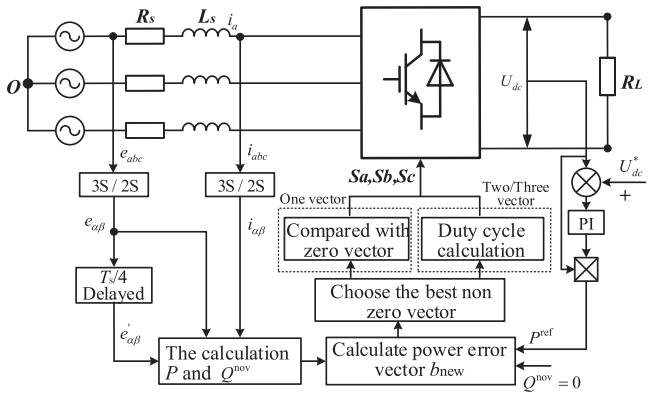

Fig. 5. Control block diagram of the proposed multivector LC-MPDPC.

DL850E. The recorded data from the DL850E is further processed in YOKOGAWA "Xviewer" software to obtain active and reactive powers, which are plotted using MATLAB. To decouple the effect of dc voltage control on performance, the PI regulator corresponding to dc voltage control is disabled in power control mode. The control block diagram of the proposed LC-MPDPC is shown in Fig. 5.

A. Performance Comparison With the Conventional MPDPC

For the sake of illustrations, the reactive power, defined by the conventional *pq* power theory, is called "imaginary power," whereas it is called "reactive power" in the extended reactive *pq* power theory. Imaginary and reactive powers are denoted by Q and Q^{nov} in this article, respectively. Experimental results for the conventional multivector LC-MPDPC and the proposed ones are demonstrated in Figs. 6 and 7. The references of active and reactive powers are 700 W and 0 Var. As shown in Figs. 6 and 7, each subfigure illustrates active power, imaginary/reactive powers, the grid voltages, and grid currents from top to bottom. The grid voltage is balanced within [0, 0.04 s], whereas it becomes unbalanced at $t = 0.04$ s. In Figs. 6(a) and 7(a), the proposed multivector LC-MPDPC and the conventional ones result in a sinusoidal grid current under balanced grid voltages. Moreover, the active and imaginary/reactive powers can track their corresponding references accurately.

Compared with the results in Figs. 6 and 7, both methods can generate sinusoidal grid current under balanced grid conditions, which demonstrates that the proposed method does not impact converter performance under balanced grid conditions. Under unbalanced grid conditions, with respect to Fig. 7, the active and imaginary powers obtained from conventional multivector LC-MPDPC can track their references accurately. However, the grid current is no longer purely sinusoidal and highly distorted when the unbalanced grid voltage occurs, and the grid current THD of both methods is close to 5.5%, i.e., 5.35% and 5.17% for two-vector- and three-vector-based LC-MPDPC using the conventional *pq* power theory. Accordingly, it exhibits not good steady-state performance.

On the other side, as shown in Fig. 6, under unbalanced grid conditions not only is the oscillation of reactive power

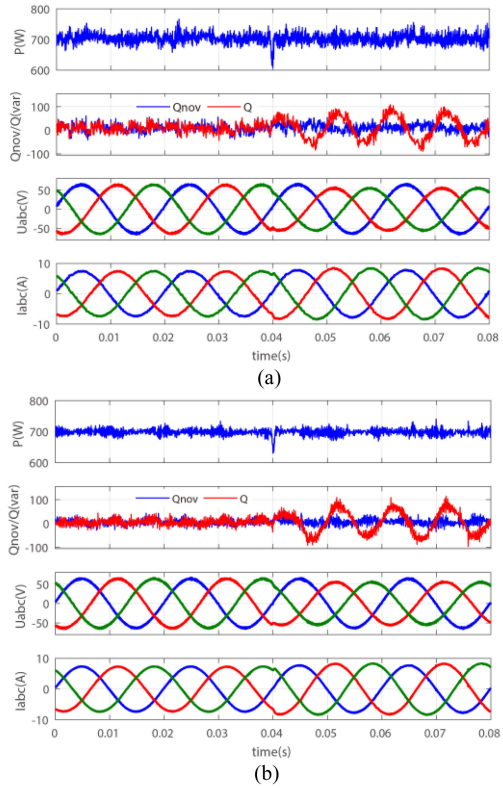

Fig. 6. Results of the LC-MPDPC using the extended *pq* power theory under 10% unbalanced grid voltages. (a) Two-vector. (b) Three-vector.

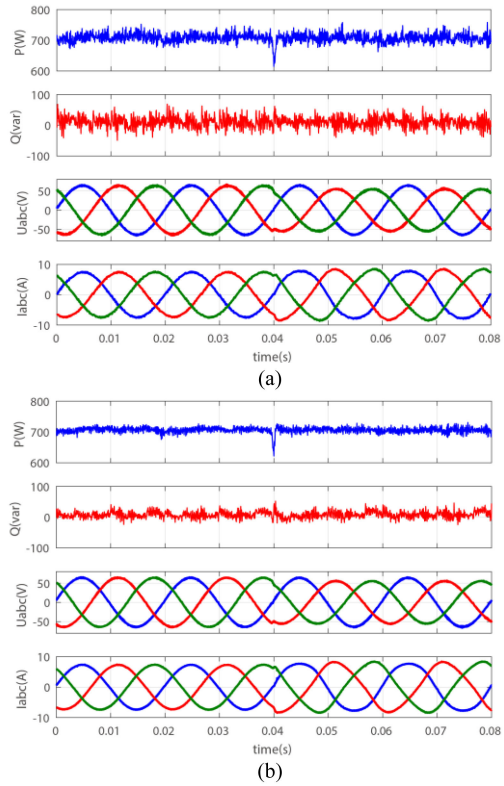

Fig. 7. Results of the LC-MPDPC using the conventional *pq* power theory under 10% unbalanced grid voltages. (a) Two-vector. (b) Three-vector.

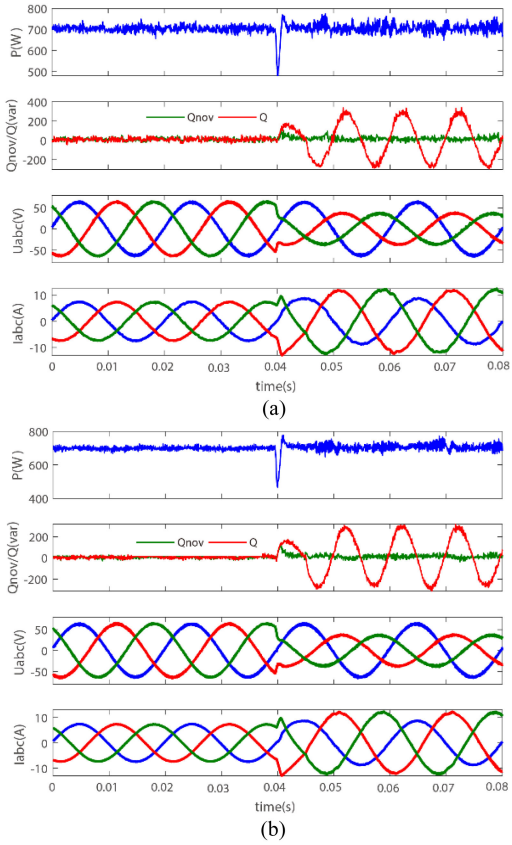

Fig. 8. Results of the LC-MPDPC using the extended *pq* power theory under 50% unbalanced grid voltages. (a) Two-vector. (b) Three-vector.

eliminated in the proposed LC-MPDPC but also the grid current is sinusoidal. Nevertheless, the imaginary power Q in the conventional *pq* power theory oscillates with the double grid frequency. Similar to the two-vector-based LC-MPDPC, a comparison with these results of three-vector-based LC-MPDPC, shown in Figs. 6(b) and 7(b), demonstrates that a better sinusoidal current is achieved using the extended reactive *pq* power theory. Consequently, a comparison between Figs. 6 and 7 demonstrates that under unbalanced grid conditions, the proposed LC-MPDPC using the extended reactive *pq* power theory is more suitable than the one using conventional *pq* power theory, as it ensures accurate reference tracking while avoiding grid current distortions under unbalanced grid conditions.

Fig. 8 describes the experimental results of the proposed LC-MPDPC using the extended *pq* power theory under 50% unbalanced grid voltages. Compared with these results of the proposed MPDPC under 10% unbalanced grid voltages shown in Fig. 6, the proposed method obtains good steady-state performance. The biggest difference is the fluctuation range of imaginary power becomes much larger because the fluctuation amplitude of imaginary power will increase with the increasing of unbalanced degree of the grid voltage [32] (see (21) in Section III).

The dynamic responses of the active and reactive powers for multivector LC-MPDPC are compared, and Fig. 9 shows the experimental results of dynamic response for the proposed

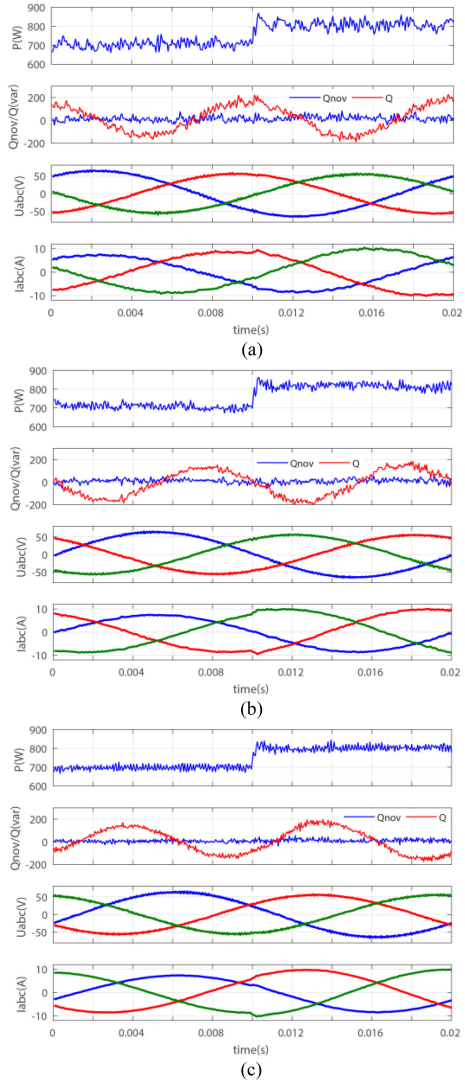

Fig. 9. Experimental results of the active power step response for the proposed LC-MPDPC. (a) One-vector. (b) Two-vector. (c) Three-vector.

multivector LC-MPDPC (one-vector- and two-vector-based methods are used as comparisons). In this scenario, the active power reference steps from 700 to 800 W, whereas reactive power remains constant. As shown in Fig. 9, during the resultant transient, the proposed three-vector-based LC-MPDPC exhibits a similar dynamic response time (0.9 ms) in tracking active power compared to one-vector- and two-vector-based LC-MPDPC method (1.0 ms), and there is no overshoot for the step response of active power. The proposed LC-MPDPC has no adverse impact on the dynamic response of the controller. Therefore, the superiority of the proposed method under unbalanced grid conditions is confirmed.

B. Performance Comparison With Multivector MPDPC

Under unbalanced grid conditions, the multivector MPDPC methods [20], [32], and [36] are proposed to reduce the power ripples or the grid current THD of rectifier, and their

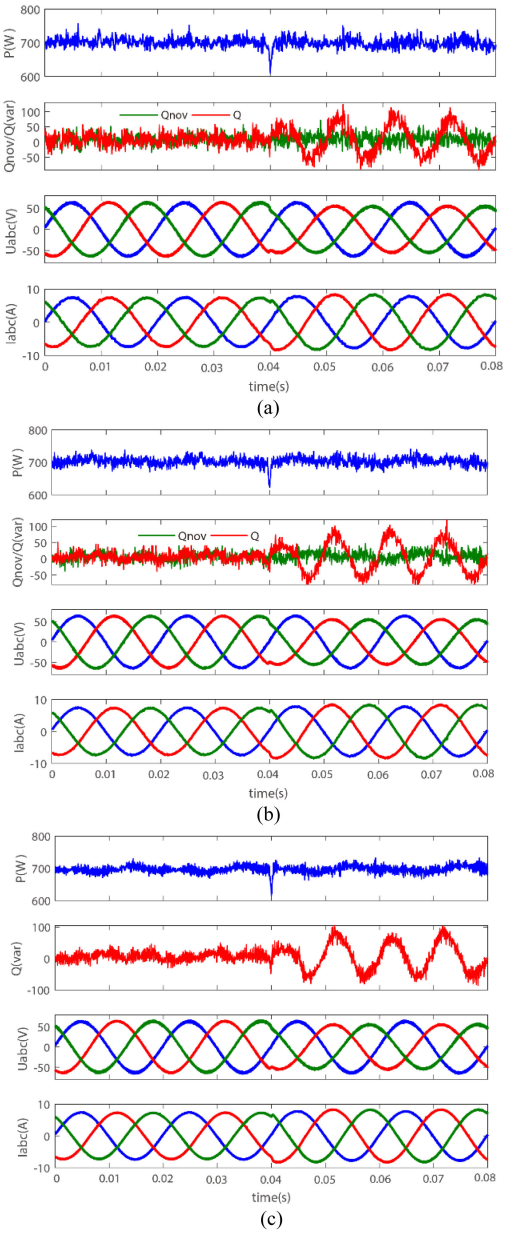

Fig. 10. Experimental results of multivector MPDPC methods. (a) MPDPC [32]. (b) UMV-MPC [36]. (c) MM-PPC [20].

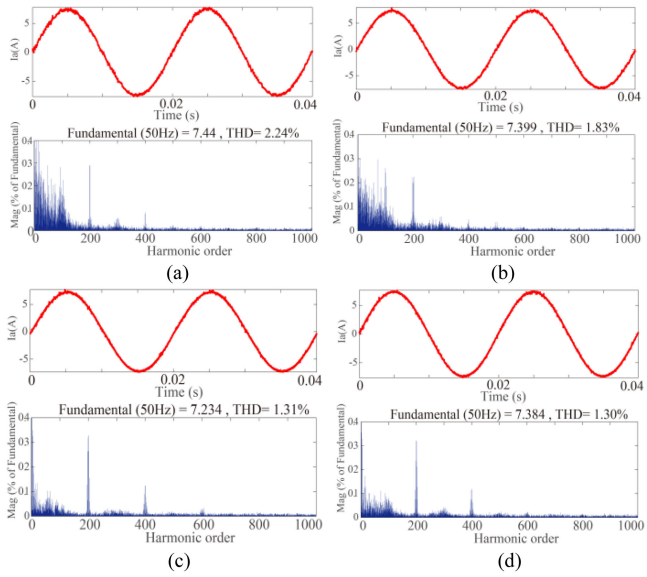

Fig. 11. Current THD results of different control methods. (a) MPDPC using the extended *pq* power theory [32]. (b) UMV-MPC [36]. (c) MM-PPC method [20]. (d) Proposed LC-MPDPC.

TABLE II
COMPARISON OF DIFFERENT PERFORMANCE

Method	MPDPC [32]	UMV-MPC [36]	MM-PPC [20]	LC-MPDPC
Sampling frequency	10 kHz	10 kHz	10 kHz	10 kHz
Switching frequency	5.31 kHz	5.29 kHz	10 kHz	10 kHz
Active PR	15.27W	13.71 W	11.32 W	11.13 W
Reactive PR	---	---	Fluctuation	---
Extended reactive PR	15.25 var	13.94 var	---	11.19 var
Current THD	2.24%	1.83%	1.31%	1.30%
Executive time(μs)	24.33 μs	17.48 μs	28.55 μs	17.93 μs

Note: "PR" denotes power ripples.

performances are compared with the proposed LC-MPDPC. The results are obtained at a 500-kHz sampling rate for fast Fourier transform to analyze grid current THD and power ripples.

Here, we only focus on performance comparisons of control methods under unbalanced grid voltages not that under balanced grid conditions. To further validate the superior performance of the proposed method, the results for [20], [32], and [36] are conducted and compared, which are shown in Fig. 10. Fig. 11 describes the grid current THD for different methods, and Table II presents the quantitative comparisons of different performances under 10% unbalanced grid voltages.

Besides, Table II presents the comparison of executive time of the proposed method and MPC method in [20], [32], and [36]. The switching frequency is computed according to the methods proposed in [20] and [29]. As listed, although the average switching frequencies of the MPDPC [32] and universal multiple-vector-based model predictive control (UMV-MPC) [36] are lower than that of the multivector model predictive power control (MM-PPC) [20] and the proposed LC-MPDPC, but power ripples of the latter ones are lower than that of the former ones, and the minimized current THD and much lower calculation complexity are achieved according to the proposed method from Table II.

Under 10% unbalanced grid voltages, the results of the presented LC-MPDPC method are shown in Fig. 6. Compared with the experimental results of other multivector MPDPC methods [20], [32], and [36] shown in Fig. 10, it is observed that much better steady-state performance is obtained using the proposed method. In the proposed LC-MPDPC, both active and reactive

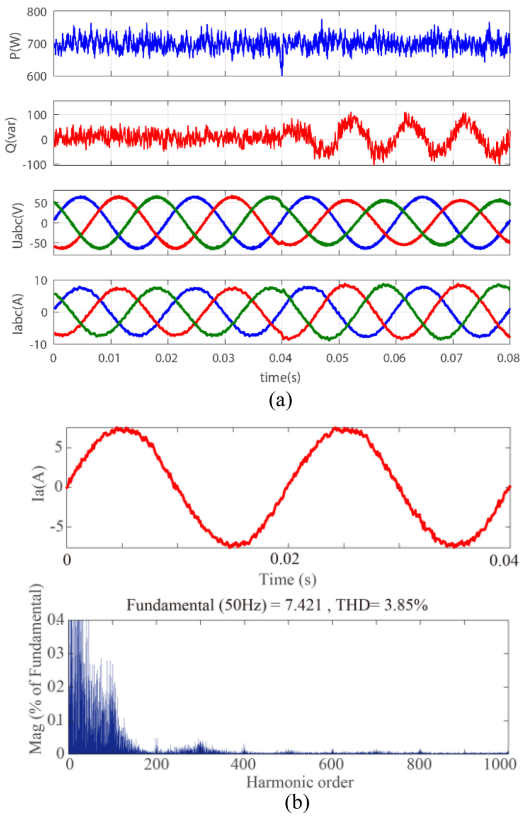

Fig. 12. Experimental results of the LC-MPDPC in [30]. (a) Active and reactive powers, the grid voltage, and grid current. (b) Grid current THD.

powers are controlled at the predefined constants, and there are lowest power ripples, i.e., 11.13 W and 11.19 var, respectively. From Fig. 11, the grid current THDs are 2.24%, 1.83%, and 1.31% for the methods, i.e, MPDPC [32], UMV-MPC [36], and MM-PPC [20], all of which are larger than that of the proposed method. Besides, by using the proposed LC-MPDPC, the grid current harmonics concentrate on the 200th-order and 400th-order harmonics, which will bring some benefits for the design of filters. Compared with MM-PPC in [20], a similar performance can be obtained using the proposed LC-MPDPC, but the executive time of the proposed method reduces from 28.55 to 17.93 μs. Accordingly, with control performance and calculation complexity, the proposed LC-MPDPC has the superior performance compared to other multivector MPDPC methods [36], [32], and [20].

C. Performance Comparison With the Existing LC-MPDPC

As described in Section I, the LC-MPDPC is studied also under balanced grid conditions in [27]–[29]. Furtherly, the LC-MPDPC in [30] is proposed under unbalanced grid voltages, which is as a comparative method in this article. Although the computational complexity is reduced, the steady-state performance needs to be further improved, which is presented in Fig. 12.

Fig. 12 describes the experimental results under unbalanced grid voltages in [30]. From Fig. 12, comparing with the experimental results obtained from the proposed method in Fig. 6, the imaginary power Q in [30] oscillates with the double grid frequency. The power ripples of active power for LC-MPDPC method in [30] and the proposed three-vector MPDPC method in this article are 20.83 and 11.13 W, respectively. Furthermore, the grid current THD corresponding to the MPC method in [30] and the proposed LC-MPDPC are 3.85% and 1.30%, respectively. Accordingly, the steady-state performance of the proposed LC-MPDPC method offers more benefits compared with the ones in [30]. Therefore, the proposed LC-MPDPC obtains much lower power ripples, and achieves much lower grid current THD under unbalanced grid voltages.

VI. Conclusion

A multivector LC-MPDPC is proposed in this article for the control of PWM rectifier under unbalanced grid conditions. Comparative experimental studies are implemented to demonstrate the effectiveness of the proposed method, which has the following features.

1) Instead of the original *pq* theory, an extended reactive *pq* theory is exploited in the proposed LC-MPDPC, in which a new complex power vector is defined. New power error is analyzed and consisted of three terms, which is described analytically in the optimal model, and its analytical expression is derived. Compared with the conventional LC-MPDPC, the proposed method obtains minimized value of cost function under unbalanced grid conditions, and also achieves good steady-state performance without changing the control structure.
2) Compared with the existing LC-MPDPC under unbalanced grid conditions, the proposed multivector method can further obtain much lower power ripples, and also lower THD for grid current without any additional power compensation. In addition, only one time is needed to predict the next voltage vector, the calculation time of the proposed method is greatly reduced. Accordingly, the proposed method can achieve good steady-state performance, and it offers a fast dynamic response and robustness under unbalanced grid conditions.

References

[1] R. Barrera-Cardenas and M. Molinas, "Comparative study of wind turbine power converters based on medium-frequency AC-link for offshore DC-grids," *IEEE J. Emerg. Sel. Topics Power Electron.*, vol. 3, no. 2, pp. 525–541, Jun. 2015.
[2] C. Meyer, M. Hoing, A. Peterson, and R. W. De Doncker, "Control and design of DC grids for offshore wind farms," *IEEE Trans. Ind. Appl.*, vol. 43, no. 6, pp. 1475–1482, Nov. 2007.
[3] N. Flourentzou, V. G. Agelidis, and G. D. Demetriades, "VSC-based HVDC power transmission systems: An overview," *IEEE Trans. Power Electron.*, vol. 24, no. 3, pp. 592–602, Mar. 2009.
[4] Z. Wang *et al.*, "A coordination control strategy of voltage-source-converter-based MTDC for offshore wind farms," *IEEE Trans. Ind. Appl.*, vol. 51, no. 4, pp. 2743–2752, Jul./Aug. 2015.
[5] H. Komurcugil, N. Altin, S. Ozdemir, and I. Sefa, "An extended Lyapunov-function-based control strategy for single-phase UPS inverters," *IEEE Trans. Power Electron.*, vol. 30, no. 7, pp. 3976–3983, Jul. 2015.
[6] J. Alonso-Martinez, J. E. Carrasco, and S. Arnaltes, "Table-based direct power control: A critical review for microgrid applications," *IEEE Trans. Power Electron.*, vol. 25, no. 12, pp. 2949–2961, Dec. 2010.

[7] P. Rioual, H. Pouliquen, and J.-P. Louis, "Regulation of a PWM rectifier in the unbalanced network state using a generalized model," *IEEE Trans. Power Electron.*, vol. 11, no. 3, pp. 495–502, May 1996.
[8] I. Villanueva, A. Rosales, P. Ponce, and A. Molina, "Grid-voltage-oriented sliding mode control for DFIG under balanced and unbalanced grid faults," *IEEE Trans. Sustain. Energy*, vol. 9, no. 3, pp. 1090–1098, Jul. 2018.
[9] Y. Zhang and C. Qu, "Table-based direct power control for three-phase AC/DC converters under unbalanced grid voltages," *IEEE Trans. Power Electron.*, vol. 30, no. 12, pp. 7090–7099, Dec. 2015.
[10] A. Sato and T. Noguchi, "Voltage-source PWM rectifier–inverter based on direct power control and its operation characteristics," *IEEE Trans. Power Electron.*, vol. 26, no. 5, pp. 1559–1567, May 2011.
[11] Y. Gui, C. Kim, C. Chung, J. M. Guerrero, Y. Guan, and J. C. Vasquez, "Improved direct power control for grid-connected voltage source converters," *IEEE Trans. Ind. Electron.*, vol. 65, no. 10, pp. 8041–8051, Oct. 2018.
[12] Y. Zhang, Z. Li, Y. Zhang, W. Xie, Z. Piao, and C. Hu, "Performance improvement of direct power control of PWM rectifier with simple calculation," *IEEE Trans. Power Electron.*, vol. 28, no. 7, pp. 3428–3437, Jul. 2013.
[13] A. Mora, Á. Orellana, and J. Juliet, "Model predictive torque control for torque ripple compensation in variable-speed PMSMs," *IEEE Trans. Ind. Electron.*, vol. 63, no. 7, pp. 4584–4592, Jul. 2016.
[14] D. Choi and K. Lee, "Dynamic performance improvement of AC/DC converter using model predictive direct power control with finite control set," *IEEE Trans. Ind. Electron.*, vol. 62, no. 2, pp. 757–767, Feb. 2015.
[15] L. Tarisciotti, G. Calzo, and A. Gaeta, "A distributed model predictive control strategy for back-to-back converters," *IEEE Trans. Ind. Electron.*, vol. 63, no. 9, pp. 5867–5878, Sep. 2016.
[16] L. Wang *et al.*, "A finite control set model predictive control method for matrix converter with zero common-mode voltage," *IEEE J. Emerg. Sel. Topics Power Electron.*, vol. 6, no. 1, pp. 327–338, Mar. 2018.
[17] Y. Zhang, W. Xie, Z. Li, and Y. Zhang, "Model predictive direct power control of a PWM rectifier with duty cycle optimization," *IEEE Trans. Power Electron.*, vol. 28, no. 11, pp. 5343–5351, Nov. 2013.
[18] Y. Zhang, D. Xu, and L. Huang, "Generalized multiple-vector-based model predictive control for PMSM drives," *IEEE Trans. Ind. Electron.*, vol. 65, no. 12, pp. 9356–9366, Dec. 2018.
[19] D. Zhou, X. Li, and Y. Tang, "Multiple-vector model-predictive power control of three-phase four-switch rectifiers with capacitor voltage balancing," *IEEE Trans. Power Electron.*, vol. 33, no. 7, pp. 5824–5835, Jul. 2018.
[20] D. Zhou, P. Tu, and Y. Tang, "Multivector model predictive power control of three-phase rectifiers with reduced power ripples under nonideal grid conditions," *IEEE Trans. Ind. Electron.*, vol. 65, no. 9, pp. 6850–6859, Sep. 2018.
[21] R. Guzman, L. Vicuna, A. Camacho, J. Miret, and J. M. Rey, "Receding-horizon model-predictive control for a three-phase VSI with an LCL filter," *IEEE Trans. Ind. Electron.*, vol. 66, no. 9, pp. 6671–6680, Sep. 2019.
[22] M. Zou, S. Wang, M. Liu, and K. Chen, "Model predictive control of permanent-magnet synchronous motor with disturbance observer," in *Proc. IEEE Int. Symp. Predictive Control Elect. Drives Power Electron.*, May 2019, pp. 1–6.
[23] F. Wang, L. He, and J. Rodrıguez, "FPGA based continuous control set model predictive current control for PMSM system using multi-step error tracking technique," *IEEE Trans. Power Electron.*, vol. 35, no. 12, pp. 13455–13464, Apr. 2020.
[24] P. Acuna, C. Rojas, R. Baidya, R. P. Aguilera, and J. E. Fletcher, "On the impact of transients on multistep model predictive control for medium-voltage drives," *IEEE Trans. Power Electron.*, vol. 34, no. 9, pp. 8342–8355, Sep. 2019.
[25] Y. Zhang, T. Jiang, and J. Jiao, "Model-free predictive current control of DFIG based on an extended state observer under unbalanced and distorted grid," *IEEE Trans. Power Electron.*, vol. 35, no. 8, pp. 8130–8139, Aug. 2020.
[26] X. Zhang, Y. Cheng, Z. Zhao, and Y. He, "Robust model predictive direct speed control for SPMSM drives based on full parameter disturbances and load observer," *IEEE Trans. Power Electron.*, vol. 35, no. 8, pp. 8361–8373, Aug. 2020.
[27] Y. Zhang and W. Xie, "Low complexity model predictive control–single vector-based approach," *IEEE Trans. Power Electron.*, vol. 29, no. 10, pp. 5532–5541, Oct. 2014.
[28] Y. Zhang, W. Xie, Z. Li, and Y. Zhang, "Low-complexity model predictive power control: Double-vector-based approach," *IEEE Trans. Ind. Electron.*, vol. 61, no. 11, pp. 5871–5880, Nov. 2014.
[29] X. Wang and D. Sun, "Three-vector-based low-complexity model predictive direct power control strategy for doubly fed induction generators," *IEEE Trans. Power Electron.*, vol. 32, no. 1, pp. 773–782, Jan. 2017.
[30] D. Sun and X. Wang, "Low-complexity model predictive direct power control for DFIG under both balanced and unbalanced grid conditions," *IEEE Trans. Ind. Electron.*, vol. 63, no. 8, pp. 5186–5196, Aug. 2016.
[31] J. Hu, J. Zhu, and D. G. Dorrell, "Predictive direct power control of doubly fed induction generators under unbalanced grid voltage conditions for power quality improvement," *IEEE Trans. Sustain. Energy*, vol. 6, no. 3, pp. 943–950, Jul. 2015.
[32] Y. Zhang and C. Qu, "Model predictive direct power control of PWM rectifiers under unbalanced network conditions," *IEEE Trans. Ind. Electron.*, vol. 62, no. 7, pp. 4011–4022, Jul. 2015.
[33] Y. Zhang and C. Qu, "Direct power control of a pulse width modulation rectifier using space vector modulation under unbalanced grid voltages," *IEEE Trans. Power Electron.*, vol. 30, no. 10, pp. 5892–5901, Oct. 2015.
[34] H. Akagi, Y. Kanazawa, and A. Nabae, "Instantaneous reactive power compensators comprising switching devices without energy storage components," *IEEE Trans. Ind. Appl.*, vol. IA-20, no. 3, pp. 625–630, May 1984.
[35] P. Cortes, J. Rodriguez, C. Silva, and A. Flores, "Delay compensation in model predictive current control of a three-phase inverter," *IEEE Trans. Ind. Electron.*, vol. 59, no. 2, pp. 1323–1325, Feb. 2012.
[36] Y. Zhang, Y. Bai, and H. Yang, "A universal multiple-vector-based model predictive control of induction motor drives," *IEEE Trans. Power Electron.*, vol. 33, no. 8, pp. 6957–6969, Aug. 2018.

Xiaohong Ran (Member, IEEE) was born in Chongqing, China. He received the Ph.D. degree in electrical power engineering from the Huazhong University of Science and Technology, Wuhan, China, in 2015.

Since 2015, he has been with the School of Electrical Engineering and Automation, Wuhan University, Wuhan, China. From 2018 to December 2021, he was a Visiting Researcher with the School of Electrical and Computer Engineering, Georgia Institute of Technology, Atlanta, GA, USA. His research interests include the control of power electronics converters applied to renewable energy technology, dc power grid/dc–dc, parameter identification, and interval optimization of power system.

Bo Xu was born in Jiangxi, China, in 1995. He received the B.S. degree in electrical engineering from Xiamen University, Xiamen, China, in 2016. He is currently working toward the Ph.D. degree in electrical engineering with Wuhan University, Wuhan, China.

His current research interests include model predictive control for power converters.

Kaipei Liu was born in Jingmen, China, in 1962. He received the Ph.D. degree in applied computer technology from Wuhan University, Wuhan, China, in 2001.

He is currently a Professor with Wuhan University. His research interests include FACTS technology, power quality control and analysis, smart grid, as well as the sustainable energy power generation and connection technologies.

Jiahao Zhang was born in Yulin, China, in 1997. He received the master's degree in electrical engineering from Wuhan University, Wuhan, China, in 2021.

He is currently with Nanning Power Supply Bureau, Guangxi Power Grid Corporation, Nanning, China. His current research interests include power system optimization model and analysis.